Received: 17 October 2017 | Revised: 4 January 2018 | Accepted: 11 January 2018

DOI: 10.1002/hbm.23981

RESEARCH ARTICLE

WILEY

Neuromodulation with single-element transcranial focused ultrasound in human thalamus

Wynn Legon | Leo Ai | Priya Bansal | Jerel K. Mueller

Division of Physical Therapy and Division of Rehabilitation Science, Department of Rehabilitation Medicine, Medical School, University of Minnesota, Minneapolis, Minnesota

Correspondence
Wynn Legon, PhD, University of Virginia, Department of Neurosurgery, 409 Lane Rd Rm. 1031, Charlottesville, VA 22908, USA.
Email: wlegon@virginia.edu

Abstract

Transcranial focused ultrasound (tFUS) has proven capable of stimulating cortical tissue in humans. tFUS confers high spatial resolutions with deep focal lengths and as such, has the potential to noninvasively modulate neural targets deep to the cortex in humans. We test the ability of single-element tFUS to noninvasively modulate unilateral thalamus in humans. Participants ($N = 40$) underwent either tFUS or sham neuromodulation targeted at the unilateral sensory thalamus that contains the ventro-posterior lateral (VPL) nucleus of thalamus. Somatosensory evoked potentials (SEPs) were recorded from scalp electrodes contralateral to median nerve stimulation. Activity of the unilateral sensory thalamus was indexed by the P14 SEP generated in the VPL nucleus and cortical somatosensory activity by subsequent inflexions of the SEP and through time/frequency analysis. Participants also under went tactile behavioral assessment during either the tFUS or sham condition in a separate experiment. A detailed acoustic model using computed tomography (CT) and magnetic resonance imaging (MRI) is also presented to assess the effect of individual skull morphology for single-element deep brain neuromodulation in humans. tFUS targeted at unilateral sensory thalamus inhibited the amplitude of the P14 SEP as compared to sham. There is evidence of translation of this effect to time windows of the EEG commensurate with SI and SII activities. These results were accompanied by alpha and beta power attenuation as well as time-locked gamma power inhibition. Furthermore, participants performed significantly worse than chance on a discrimination task during tFUS stimulation.

KEYWORDS

human, neuromodulation, somatosensory, thalamus, transcranial, ultrasound

1 | INTRODUCTION

Current noninvasive neuromodulatory approaches like transcranial magnetic stimulation (TMS) and transcranial direct current stimulation (tDCS) have proven capable for inducing transient plastic changes in the human cortex. Despite their wide employment, these technologies are limited. They have poor spatial resolution, suffer from a depth focality tradeoff, and experience significant attenuation at depth (Deng, Lisanby, & Peterchev, 2014). Thus, they cannot effectively target neural tissue below the surface of the cortex. tFUS is a new and very promising nonsurgical low-energy technique for inducing transient plasticity with high spatial resolution and adjustable focus (Legon et al., 2014), capable of targeting deep neural structures. tFUS has been used safely and effectively for cortical neuromodulation in mouse (Kim, Chiu, Lee, Fischer, & Yoo, 2014; King, Brown, Newsome, & Pauly, 2013; Mehic et al., 2014; Moore, Loft, Clegern, & Wisor, 2015; Tufail et al., 2010), rabbit (Yoo et al., 2011), pig (Dallapiazza et al., 2017), and monkey (Deffieux et al., 2013) and research has shown tFUS to also be a safe and effective method of transient cortical stimulation in humans (Lee et al., 2015; Lee, Chung, Jung, Song, & Yoo, 2016a; Lee et al., 2016b; Legon et al., 2014; Mueller, Legon, Opitz, Sato, & Tyler, 2014). We demonstrated single-element ultrasound can inhibit the amplitude of somatosensory evoked potentials (SEPs) when targeted at the cortical regions that generate these potentials. The lateral resolution of the pressure field of a single element transducer is less than the width of a human gyrus allowing for detailed targeting (Legon et al., 2014). Translation of the acoustic field only 1 cm from the original effective target site removed the modulatory effect (Legon et al., 2014). We have shown

that single element ultrasound is safe and easily employable in humans and effective for transient cortical neuromodulation but one of the great advantages of ultrasound (its deep focal lengths) has not been systematically tested in humans. Previous reports have used single element ultrasound for neuromodulation of deep brain structures in different animal models. For example, Min et al. (2011) and Yang et al. (2012) applied low intensity single element ultrasound to the thalamus in rat and reported changes in frontal lobe neurotransmitter concentrations though did not report data from thalamus (Min et al., 2011; Yang et al., 2012). Downs, Buch, Karakatsani, Konofagou, and Ferrera (2015) directed single element focused ultrasound at thalamus in awake behaving primate and showed ultrasound (with the addition of microbubble contrast) to safely disrupt the blood–brain barrier (Downs et al., 2015). These studies provide initial evidence of the ability of single element ultrasound to target the thalamus though these studies did not expressly study the use of ultrasound for thalamic neuromodulation. In a recent report, Dallapiazza et al. (2017) demonstrated the ability of 1.14 MHz low intensity focused ultrasound to target specific nuclei within thalamus in craniotomized pig resulting in inhibited SEPs (Dallapiazza et al., 2017). These results are very encouraging for the use of single element ultrasound for deep brain stimulation that may be feasible in human though this has not yet been demonstrated. There is a case report of single-element ultrasound directed at the thalamus in a TBI patient though no physiological data or otherwise is provided (Monti, Schnakers, Korb, Bystritsky, & Vespa, 2016). As such, it is the purpose of this study to target the unilateral thalamus in humans with noninvasive tFUS and record the direct effect on thalamus as evidenced by the amplitude of the P14 somatosensory evoked potential (SEP). The effect of tFUS to thalamus on cortical somatosensory regions is also examined as well as effect on behavior using a tactile judgement task.

2 | MATERIALS AND METHODS

2.1 | Experimental procedures

2.1.1 | Participants

The Institutional Review Board at the University of Minnesota approved all experimental procedures. Forty volunteer study participants (14 male, 26 female, aged 18–37 with a mean age of 23.0 ± 4.38 years) provided written informed consent to participate in either the EEG or behavioral portion of the study. All participants were self-reported right handed, and none of the participants reported any neurological impairment or identified any contraindications to noninvasive neuromodulation as outlined by Rossi et al. (2009) for transcranial magnetic stimulation.

Participants were seated in a dentist type chair with their right forearm and elbow fully supported in supination. During testing, subjects were required to sit passively while viewing a fixation cross on a screen. A total of 300 ultrasonic waveforms (see below) were delivered at an inter-stimulus interval (ISI) of 4 s. The tFUS condition involved acoustically coupling the active face of the ultrasound transducer to the scalp at the predetermined neuronavigation site (see *tFUS targeting* below). The sham condition involved placing a high acoustic impedance disk on the face of the transducer. This maintained contact of the transducer to the head to mimic the audible sensation of a slight buzzing but attenuate any energy into the head. The audible sound was identical for both the sham and tFUS conditions and no subjects reported any sensory or perceptual differences between the two conditions. The presence of tactile stimulation of the skin is possible using 0.5 MHz ultrasound though the focus would need to be in the skin and of sufficient intensity (>16 W/cm^2) (Gavrilov, 2016), thus making the presence of scalp tactile stimulation unlikely in this case given the deep focal lengths of the transducer used and thus the nominal pressures generated at the scalp. The order of sham or tFUS conditions was randomized for each subject with a 10-min break time between conditions. Total collection time was ~1 h.

2.1.2 | tFUS targeting

The transducer cavity was filled and sealed with acoustic coupling gel and placed on the scalp after parting of the hair and administration of addition gel, using a neuronavigation system (BrainSight, Rogue Research, Montreal, QUE, CAN). Individual subject anatomical MRI acquired prior to tFUS testing was retrofitted to work with the ultrasound transducers that takes into consideration the focal length of the transducer so that the spatial peak of the ultrasound beam targeted the left hemisphere somatosensory nuclei as defined by Behrens et al (2003) using diffusion imaging. Individual participant targets were transformed from MNI space to individual space using the FSL flirt command (https://fsl.fmrib.ox.ac.uk). Optimal positioning was at the side of head above the ear through the temporal window for all participants (Figure 1a). The transducer was secured to the head and positioning verified online throughout the experiment using the neuronavigation system.

2.1.3 | MR acquisition

MRI data were acquired on a Siemens 3T Prisma scanner (Siemens Medical Solutions, Erlangen, Germany) at the University of Minnesota's Center for Magnetic Resonance Research. Anatomical scans were acquired using a T1 weighted MPRAGE sequence with the following parameters: TR = 2,400 ms, TI = 1,060 ms, TE = 2.12 ms, flip angle = 8°, voxel size = 1 mm isotropic, matrix size = 256 × 256, 192 slices.

2.1.4 | tFUS waveform

Transcranial ultrasonic neuromodulation waveforms were generated using a two-channel, 2-MHz function generator (BK 4078B Precision Instruments). Channel 1 was used to gate channel 2 that was a 500 kHz sine wave. Channel 1 was a 5Vp-p square wave burst of 1 kHz (N = 500) with a pulse width of 360 μs. This resulted in a 0.5 s duration waveform with a duty cycle of 36% (Figure 1b). The output of channel 2 was sent through a 100-W linear RF amplifier (E&I 2100L; Electronics & Innovation) before being sent to a custom-designed focused ultrasound transducer (Ultran Group, Inc., State College, PA)

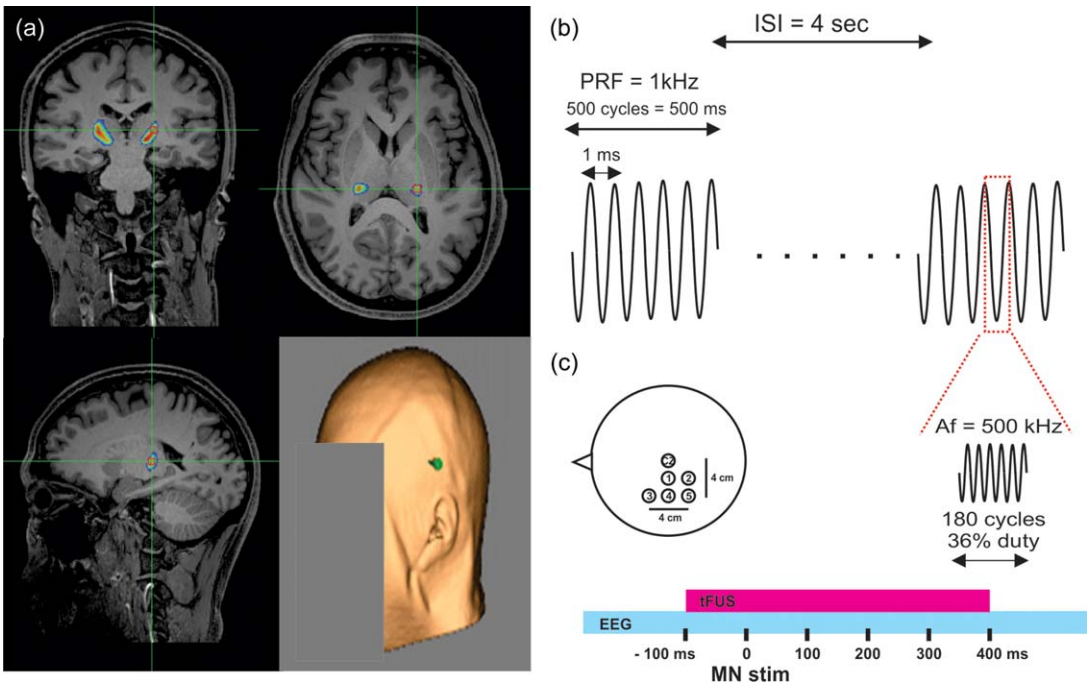

FIGURE 1 Targeting and application of tFUS. (a) Anatomical MRI showing overlaid targeted somatosensory volume in pseudocolor at green cross hairs taken from Behrens et al. (2003). Bottom right shows the typical center of transducer placement (green point) on individual subject scalp rendering from MRI anatomical image. (b) Schematic of the ultrasound pulsing strategy. ISI = interstimulus interval; PRF = pulse repetition frequency; Af = acoustic frequency. (c) Schematic of the position of the 5 electrodes on the scalp referenced in space to electrode CZ at vertex. Electrodes were spaced from CZ at 2 cm increments. Bottom represents the timing of transcranial focused ultrasound (tFUS) application relative to median nerve stimulation (MN stim). EEG represents continuous electroencephalographic recording from the 5 scalp electrodes

having a center frequency of 0.5 MHz, 63 mm aperture, 70.92 mm focal length (55 mm from exit plane), and an f# of 1.13.

2.1.5 | Electroencephalography

Electroencephalography (EEG) data were acquired using a DC amplifier (Electrical Geodesics Inc., OR, USA) with five 10-mm gold-over-silver cup electrodes placed at scalp sites spaced by 2 cm relative to the vertex (CZ) to cover the sensorimotor cortex referenced to the bilateral mastoid and grounded to the left ulnar styloid process (Figure 1c). Cup electrodes were filled with a conductive paste (Ten20 Conductive; Weaver and Company, Aurora, CO) and held in place with tape. The scalp was first prepared with a mild abrasive gel (Nuprep; Weaver and Company, Aurora, CO) and rubbing alcohol. Electrode impedances were verified (<50 kΩ) before recording. EEG data were online filtered (DC–200 Hz) and digitized at 1,000 Hz before being stored on a computer for offline analysis. Somatosensory evoked potentials (SEPs) were elicited in response to right median nerve stimulation using a 0.2-ms square-wave pulse driven by an SD-9 stimulator (Grass Technologies, Warick, RI) delivered through a bar electrode (2 cm electrode spacing) affixed to the wrist. Intensity was adjusted to elicit a slight twitch of the thumb. Stimuli were delivered at an average interstimulus interval of 4 s. For each condition, a total of 300 MN stimuli were delivered. Median nerve stimuli were time-locked to occur 100 ms after the onset of tFUS waveforms (Figure 1c).

2.1.6 | Statistical analysis of somatosensory evoked potentials

EEG data were preprocessed using custom scripts written in Matlab v7.14.0.739 (R2012a) (The MathWorks, Inc., Natick, MA). Data were band-pass filtered (2–180 Hz) using a third-order Butterworth, epoched around median nerve stimulus (−200 to 500 ms) and baseline corrected (−200 to −100 ms). Data were manually inspected for artifact (eye blink, muscle activity) and contaminated epochs removed. The maximum number of rejected trials for a single participant was 32. As such, SEPs for each subject for each condition were the result of 268 randomly selected trials to equate trials between conditions and participants. Two forms of SEP waveform analysis were employed: time series analysis and peak-to-peak analysis. For time series analysis, traces for each channel were analyzed using nonparametric permutation statistics ($p < .05$; 2,000 randomizations) which appropriately control for multiple comparisons problems encountered in analyses of complex EEG data sets (Maris & Oostenveld, 2007), where statistical *P* values represent the proportion of 2,000 random partitions resulting in a test statistic larger than the *t* value calculated by a conventional paired *t*-test (two-tailed, d.f. = 19) on the data. In addition, a temporal cluster threshold of at least 3 consecutive time-points was required to satisfy significance. For peak-to-peak analysis, waveform peak amplitude and latency were manually identified and quantified using custom scripts written in Matlab. All classically defined SEP components were assessed. This included the P14, N20, P27, N33, P50, N70, P100,

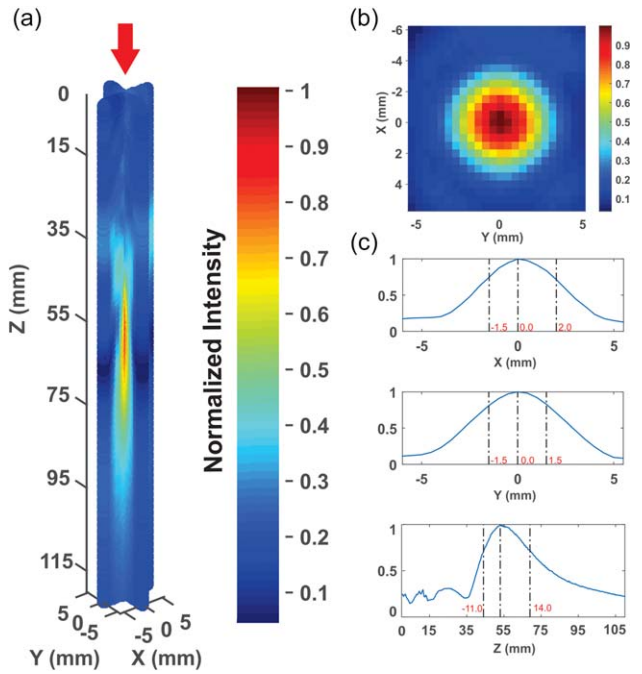

FIGURE 2 Ultrasound beam characteristics. (a) Normalized 3D pseudocolor empirical plot of ultrasound beam recorded in free water. Maximum I_{sppa} in free water was 14.56 W/cm^2 with an MI of 0.89 and 7.03 W/cm^2 measured through a sectioned human temporal bone. (b) Normalized pseudocolor empirical plot of XY lateral resolution (taken at Z maximum) of ultrasound in free water. (c) *X*, *Y*, and *Z* normalized line plots of pressure profiles normalized to peak pressure. Dashed lines and red numbers indicate −3 dB pressure attenuation in respective axes

N140, and late potential (LP) (Allison et al., 1989a; Allison, McCarthy, Wood, Williamson, & Spencer, 1989b). A distinct inflection of the waveform was necessary for inclusion in statistical analyses. Statistical analyses were performed on mean (268 trials) peak-to-peak amplitudes differences for the P14/N20, N20/P27, N33/P27, P50/N33, N70/P50, P100/N70, N140/P100, and LP/N140 components of SEPs recorded during sham and tFUS conditions ($n = 20$ subjects). Peak-to-peak amplitudes for each peak of interest were analyzed using paired *t* tests to test for differences between ultrasound and sham neuromodulation. To control for multiple comparisons across channels, a *p* value of 0.05/5 channels was considered statistically significant. Values for SEP amplitudes are reported as mean ± s.e.m.

2.1.7 | Frequency decomposition

The fast Fourier transform was applied using custom scripts written in Matlab v7.14.0.739 (R2012a) (The MathWorks, Inc., Natick, MA) for the time epoch 10–300 ms for the frequencies 8–80 Hz. Data were zero-padded to increase frequency resolution to 2 Hz. For Morlet wavelet convolution, the time window −800 to 800 ms was used to avoid edge artifacts in the desired time window (−100 to 300 ms). Sixty total frequencies were used ranging from 8 to 200 Hz. Data are displayed in 8–80 Hz. A range of 4–20 wavelet cycles were used that were log-spaced with the number of frequencies. Data were baseline subtracted from time window −200 to −500 ms.

2.1.8 | Statistical analysis spectral content

FFT data were treated as a time-series and analyzed using permutation statistics as reported above for EEG data (1,000 repetitions, $p < .05$) with a temporal cluster threshold of 2 consecutive time-points. Wavelet data were similarly analyzed using two-dimensional permutation statistics (2,000 randomizations, $p < .05$, 3 contiguous 2D cluster threshold). Wavelet data are presented as decibel (dB) change relative to baseline window (−200 to −500 ms).

2.1.9 | Empirical acoustic field mapping

We measured the acoustic intensity profile of the waveform in an acoustic test tank filled with deionized, degassed, and filtered water (Precision Acoustics Ltd., Dorchester, Dorset, UK). A calibrated hydrophone (HNR-0500, Onda Corp., Sunnyvale, CA, USA) mounted on a motorized stage was used to measure the acoustic intensity profile from the ultrasound transducer in the acoustic test tank at a 100 μm spatial resolution (Figure 2). Intensity parameters were derived from measured values of pressure using the approximation of plane progressive acoustic radiation waves (Preston, 1986). A detailed discussion of the effect of such approximations to calculate intensity can be found in Beissner (1982). The ultrasound transducer was positioned in the tank using optomechanical components (Edmund Optics Inc., Barrington, NJ and Thorlabs Inc., Newton, NJ). Acoustic field scans were performed in the free water and through hydrated sectioned human temporal bone.

2.2 | Quantitative modeling of ultrasound wave propagation

Computational models were developed using images from magnetic resonance (MR) imaging and computerized tomography (CT) of individuals to evaluate the wave propagation of tFUS across the skull and the resultant intracranial acoustic pressure maps. Simulations were performed using the k-Wave MATLAB toolbox (Treeby & Cox, 2010), which uses a pseudospectral time domain method to solve discretized wave equations on a spatial grid. Acoustic simulations using k-Wave were used on one male model constructed using datasets from the Visible Human Project® (Spitzer & Whitlock, 1998). Each dataset consists of MR, CT and cryosection images taken in the axial plane of the head at various slice thicknesses (4 mm MR, 1 mm CT). CT images were used to construct the acoustic model of the skull, while MR images were used to target tFUS at the unilateral sensory thalamus based upon individual brain morphology. Details of the modelling parameters can be found in Mueller, Ai, Bansal, and Legon (2017).

CT and MR images were first co-registered in MATLAB to guide targeting of ultrasound to the unilateral sensory thalamus. The images were then resampled for acoustic simulations at a finer resolution and the acoustic parameters for simulation calculated from the CT images. The skull was extracted manually using a threshold intensity value and the intracranial space was assumed to be homogenous as ultrasound reflections between soft tissues are small (Mueller, Ai, Bansal, & Legon, 2016). Acoustic parameters were calculated from CT data assuming a linear relationship between skull porosity and the acoustic parameters (Aubry, Tanter, Pernot, Thomas, & Fink, 2003; Marquet et al., 2009).

TABLE 1 Acoustic parameters

Speed of sound ($m\ s^{-1}$)	Density ($kg\ m^{-3}$)	Absorption ($Np\ MHz^{-1}\ m^{-1}$)
$c_{water} = 1482$	$\rho_{water} = 1000$	$\alpha_{water} = 3.48e\text{-}4$
$c_{bone,c} = 3100$	$\rho_{bone} = 2200$	$\alpha_{min,skull,c} = 21.5$
$c_{bulk} = 2850$	$\rho_{bulk} = 1732$	$\alpha_{max,skull,c} = 208.9$
		$\alpha_{bulk} = 85.0$

Simulations were then carried out using software and services provided by the Minnesota Supercomputing Institute at the University of Minnesota. The computational model of the ultrasound transducer used in simulations was constructed to recreate empirical acoustic pressure maps of focused ultrasound transmitted in an acoustic test tank, similar to previous work (Mueller et al., 2016). The ultrasound transducer modeled was the transducer used in the EEG and behavioral experiments. The transcranial ultrasonic neuromodulation waveform that the simulations were based on is as stated above and has been previously described (Legon et al., 2014). Skull models were considered to be immersed in water to couple the model to the ultrasound source. The acoustic properties of the skull model were calculated from CT Hounsfield units (H) based on a porosity (ψ) calculated using Equation 1 (Aubry et al., 2003; Marquet et al., 2009). Following calculation of porosity, the compressional speed of sound ($c_{skull,c}$), density (ρ_{skull}), and attenuation ($\alpha_{skull,c}$) of the skull were calculated using Equations 2–4 (Aubry et al., 2003; Marquet et al., 2009) with the parameters given in Table 1. The minimum and maximum compressional attenuation of skull was taken from Connor (2003) and corresponds to the extreme values of absorption listed at 500 kHz. The attenuation of water was calculated for a frequency of 500 kHz at 37°C, corresponding to body temperature, using the built-in function in k-Wave based on previous literature (Pinkerton, 1949).

$$\psi = 1 - \frac{H}{1000} \tag{1}$$

$$c_{skull,c} = c_{water}\psi + c_{bone,c}(1-\psi) \tag{2}$$

$$\rho_{skull} = \rho_{water}\psi + \rho_{bone}(1-\psi) \tag{3}$$

$$\alpha_{skull,c} = \alpha_{min,skull,c} + (\alpha_{max,skull,c} - \alpha_{min,skull,c})\psi^{0.5} \tag{4}$$

A spatial discretization of 7 points per wavelength in water (0.42 mm) was chosen for our simulations, which results in simulation domains for the baseline model of ~500 × 500 × 500 grid points. A Courant–Friedrichs–Lewy stability criterion (CFL number) of 0.1 and the default 115 cycles were used for all simulations.

2.3 | Behavioral assessment of tFUS

Twenty volunteer participants (6 male, aged 18–33 with a mean age of 22.6 ± 4.8 years) provided written informed consent to participate in the study. None of the volunteers reported any neurological impairment and all were self-reported as right-hand dominant.

2.4 | Experimental setup

Behavioral assessment was identical to Legon et al. (2014). Subjects were seated in a dentist type chair with their right arm resting on a tabletop with the pad of their index finger resting over a 1.1 × 1.9 cm oval through which stimuli were delivered. A total of nine pin (pin diameter = 200 μm) separation distances were used including 0, 0.7, 1.0, 1.3, 1.6, 1.9, 2.2, 2.5, and 2.8 mm. Each pin distance was randomly applied at a constant force of 1 N to the fingertip 10 times during tFUS or sham condition. After each stimulus, participants were required to report verbally whether they felt one or two pins. Before formal testing, participants were familiarized with the sensations produced by pins separated by 0 (one pin), 1.6, and 2.8 mm and informed after each stimulus to the fingertip whether the stimulus was one or two pins. Practice sessions of 5 trials of each pin distance (0, 1.6, and 2.8) were conducted. Formal testing began once participants achieved 80% (4/5) correct responses in response to stimulation using 0 and 2.8 mm pin distances. Participants were not aware of how many pin distances were used or the ratio of single to double pins during formal testing. Participants were not allowed to look at their fingers, but they were allowed to have their eyes open or closed. It was not possible for the participant to see the pins, as they were occluded from view under a table. A custom-made motorized device that was controlled by custom-made software (LabVIEW, National Instruments, Austin, TX) was built to apply the pin to the fingertip. This allowed for precisely controlled force (1 N) and duration (250 ms) of the pins to the fingertip. The software also timed the onset of tFUS (500 ms duration) to occur 100 ms before the pin application to the fingertip. Participants underwent the sensory discrimination testing during both tFUS and sham conditions in the same testing session. The order of sham or tFUS was counterbalanced across subjects. Total collection time was ~1 h.

2.5 | Statistical analysis

Based on previous results (Legon et al., 2014) that demonstrated effects at subjective threshold, we blocked the 9 pin separations into 3 general categories: catch trials (0 mm), hard discrimination (0.7–1.3 mm), and easy discrimination (2.2–2.8 mm). Data (% correct) from the pin separations in hard and easy categories were collapsed and averaged for each of the tFUS and Sham conditions. Differences between tFUS and Sham were tested for each category using paired t tests. To control for multiple comparisons, a p value of 0.05/3 was considered statistically significant. Both tFUS and Sham data for the threshold category were tested against chance using a one-way t test with mean 0.5.

3 | RESULTS

3.1 | Ultrasound waveform

Measurements in the acoustic tank revealed an I_{sppa} of 14.56 W/cm^2 and an MI of 0.89 from the ultrasonic neuromodulation waveform in water, and 7.03 W/cm^2, MI of 0.56 when transmitted through the temporal window of the sectioned skull. The focal length of the transducer

TABLE 2 Distance to unilateral thalamus

	Mean (mm)	SD (mm)	Max (mm)	Min (mm)
Female ($N = 26$)	56.57	2.41	60.6	52.1
Male ($N = 14$)	59.88	2.36	65.3	53.1
All ($N = 40$)	57.62	2.83	65.3	52.1

was 55 mm from the exit plane and the −3 dB pressure attenuation was 3.5 mm in the *x*-axis, 3.0 mm in the *y*-axis, and 25 mm in the *z*-axis (Figure 2). We have previously verified that similar waveforms do not produce appreciable heating of the skin or skull bone (Mueller et al., 2016).

3.2 | Ultrasound targeting

Optimal transducer positioning was always at the side of the head based upon the focal length of the transducer and the depth of thalamic target to the scalp. Table 2 lists the depth of the targeted thalamic region for all 40 participants. The average distance from the scalp was 56.57 ± 2.41 mm for females and 59.88 ± 2.36 for males. For the group ($N = 40$), the minimum distance from the scalp was 52.1 mm and the maximum was 65.3 mm (Table 2).

3.3 | Electroencephalography

We targeted the unilateral sensory nuclei of thalamus using a single element focused ultrasound transducer. The VPL nucleus contains a synapse in the dorsal column medial lemniscal system that can be recorded noninvasively as the P14 of the scalp electroencephalographic (EEG) somatosensory evoked potential (SEP) (Katayama & Tsubokawa, 1987). We continuously recorded EEG from 5 scalp electrodes positioned over the left hemisphere during ultrasound neuromodulation and during a sham condition. Grand average ($N = 20$) SEPs are shown in Figure 3b from the five channel recordings. To fully characterize the effect of tFUS on the EEG we performed nonparametric permutation time series analysis (Maris & Oostenveld, 2007) as well as peak-to-peak SEP amplitude analysis. We found that ultrasound to the left unilateral sensory thalamus reliably attenuated the amplitude of the EEG time series at latencies between 14 and 21 ms during the tFUS condition as evidenced in channels 1–4 ($p < .05$ corrected) (Figure 3b). In addition, tFUS inhibited the early negativity around 35 ms in these channels ($p < .05$ corrected) (Figure 3b) and also demonstrated an increase in positivity of the large late negative/positive inflection around 140–200 ms ($p < .05$ corrected) (Figure 3b). Peak-to-peak amplitude analysis of established peaks of the SEP (Allison, McCarthy, Wood, & Jones, 1991) revealed a strong attenuation of the P14/N20 complex for the tFUS condition ($t = -3.28$, df = 19, $p < .004$ paired *t*-test) in all channels (Figure 3a) supporting the time-series analyses. No other peak-to-peak pair reached the corrected significance though the N33–P27 showed a trend for suppression ($p = .05$) in channel 3 and 4 mirroring the time series analysis (Supporting Information, Figure 1) and the N140–P100 peak-to-peak pair also showed a trend for tFUS inhibition ($p = 0.06$) in channel 2 (Supporting Information, Figure 1). There was no effect of tFUS on the latency of any of the recorded potentials (Supporting Information, Figure 2).

To more comprehensively understand the effect of tFUS on the EEG, we performed frequency decomposition using the fast Fourier transform (FFT) and the Morlet wavelet convolution. FFT provides an overall assessment of frequency power for the entire time epoch, whereas Morlet wavelet convolution provides for precise timing of power change within the time epoch providing complimentary analysis of group time-locked activity changes as a result of tFUS. The FFT

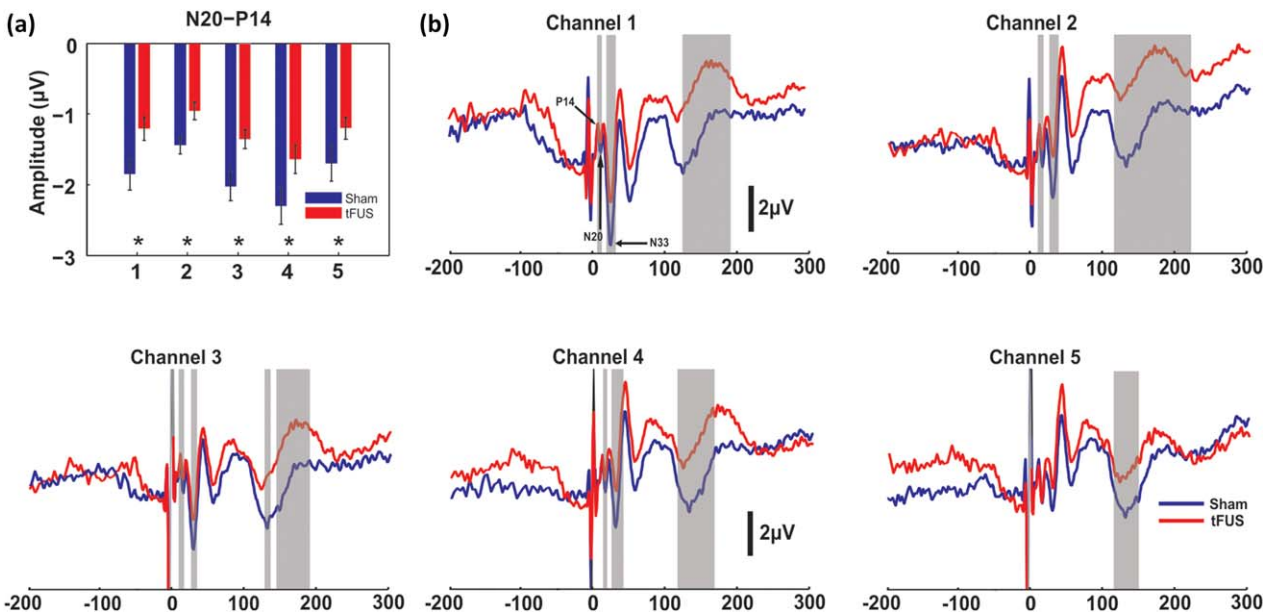

FIGURE 3 Group average somatosensory evoked potentials. (a) Group mean ($n = 20$) peak-to-peak amplitude of the N20-P14 SEP for 5 channel recordings. * denotes $p < .01$. Bars represent ± SEM. (b) Group average ($n = 20$) somatosensory evoked potential (SEP) traces recorded from 5 scalp EEG channels. Vertical grey bars denote time windows that met statistical significance ($p < .05$ corrected)

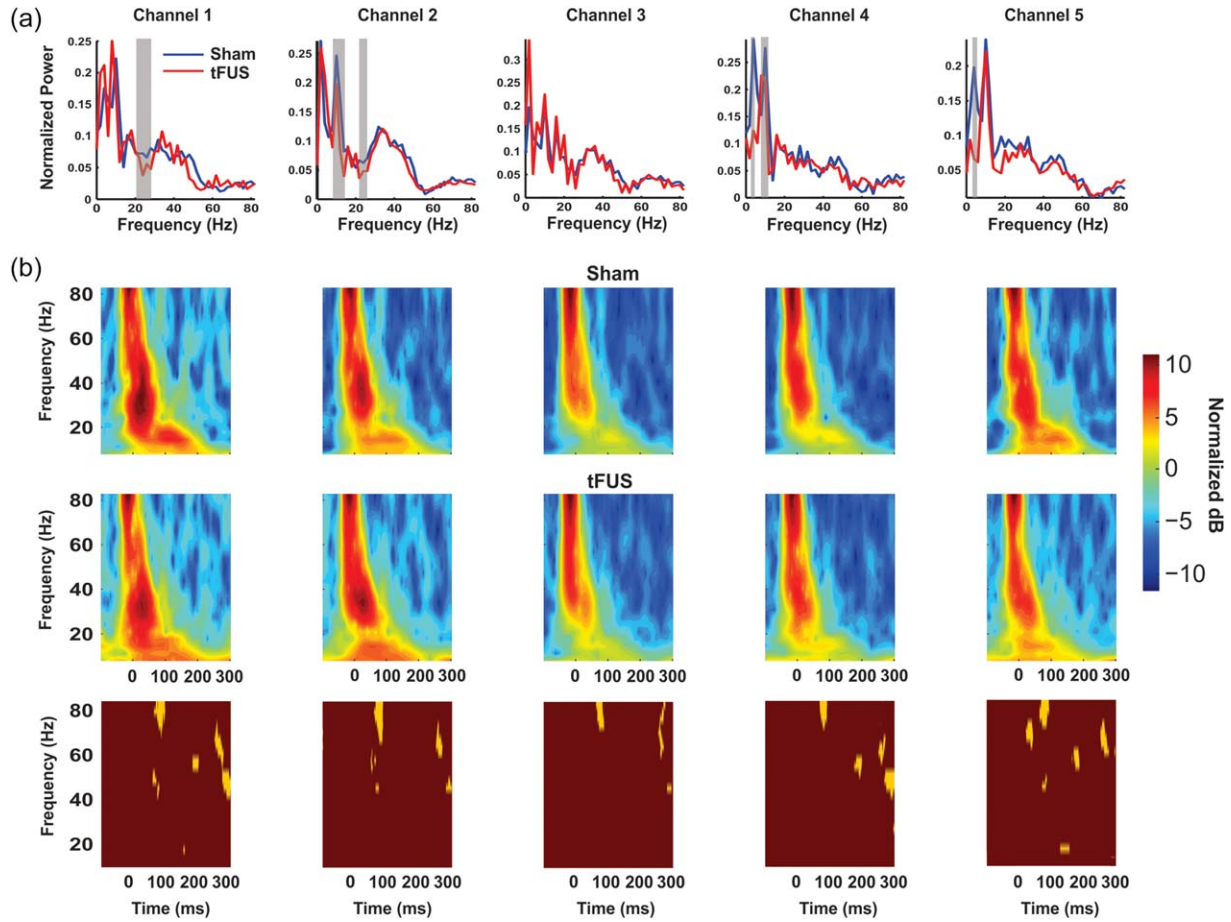

FIGURE 4 Group average frequency spectra. (a) Group mean ($n = 20$) FFT frequency spectra for EEG time window 10–300 ms post MN stimulation. Vertical grey bars denote time widows that met statistical significance ($p < .05$ corrected). (b) Group mean pseudocolor ($n = 20$) Morlet wavelet time–frequency spectra in decibels (dB) relative to a prestimulus baseline. Top row is Sham stimulation and middle row is ultrasound (tFUS) stimulation. Gold and maroon boxes (bottom row) are statistical maps of time–frequency data; gold areas met statistical significance ($p < .05$ corrected)

revealed tFUS to result in a decrease in power of frequencies in the alpha range (7–13 Hz; $p < .05$ corrected) in channels 2, 4, and 5 and attenuation of beta amplitude (20–30 Hz; $p < .05$ corrected) in channels 1 and 2 (Figure 4a). Wavelet analysis revealed a consistent decrease in gamma power (~80 Hz) during tFUS around 100 ms in all channels ($p < .05$) (Figure 4b) and late >200 ms gamma attenuation. There was little evidence for time-locked alpha or beta attenuation.

3.4 | Behavior

To understand if these electrophysiologic results translate to behavioral effects, we had a separate group of participants ($N = 20$) perform a two point discrimination task during either tFUS or sham neuromodulation. All participants performed the discrimination task well (97% and 98% correct on catch trials for tFUS and sham respectively) (Figure 5a). Easy and hard discriminations were performed equally well for both tFUS and sham conditions (easy: tFUS 93%, Sham 96% correct; hard: tFUS 23%, Sham 22% correct) (Figure 5a). Differences emerged for threshold discriminations. There was a slight decrease in performance for the tFUS group as compared to sham that did not reach statistical significance as compared to sham neuromodulation (tFUS: 43.5% correct; Sham 53.33% correct: $t = -1.73$, df = 29, $p = .074$) (Figure 5a). However, the tFUS group did perform significantly worse than chance for these threshold tests whereas the sham group performed at chance. (tFUS = 43.5%; one-sided t test, $t = -2.071$, $p = .0474$; Sham = 53.33%; one-sided t-test, $t = 0.52$, $p > .05$) (Figure 5b).

3.5 | Acoustic simulations

Simulations were run on a Visible Human Project® male dataset using CT and MRI images to accurately assess the effect of individual skull morphology on ultrasound wave propagation for deep brain neuromodulation. In Figure 6, we show the wave propagation as projected from the side of the head. There is good reservation of the ultrasound beam profile as compared to the free water empirical tank observations; though there is evidence of additional side lobes and some beam distortion when taking the skull into consideration (Figure 6). In this model, the skull reduced the intracranial max acoustic pressure to 137.79 kPa representing a reduced peak pressure produced by the transducer in free water by six- to sevenfold.

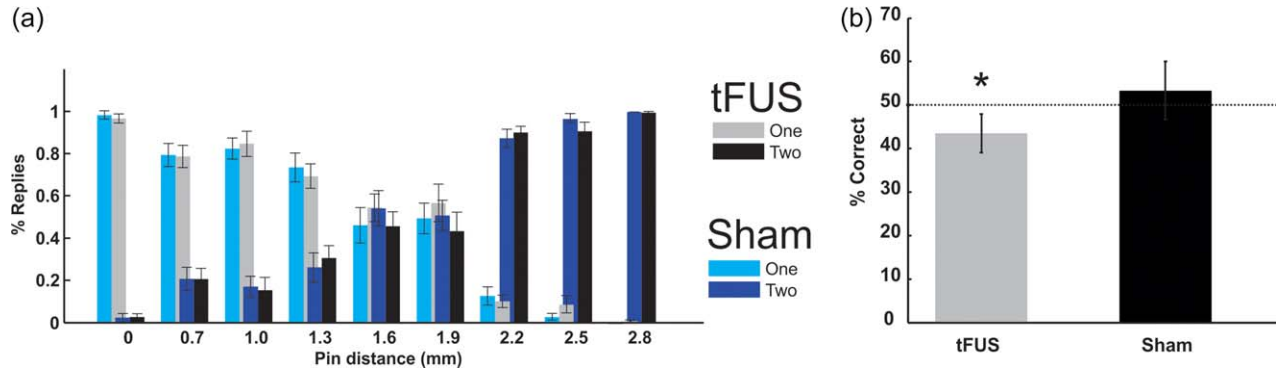

FIGURE 5 Group average behavioral results. (a) Group average ($n = 20$) two point discrimination behavior for tFUS condition (black and grey) and sham condition (light and dark blue). Light bars (grey and light blue) for each condition denotes % of trials where subjects verbally responded they felt one pin, and dark bars (black and dark blue) denote % of trials where subjects reported feeling two pins. Catch trials with only one pin is denoted with 0 on *x*-axis. (b) Collapsed data from 1.6 and 1.9 mm separations as percent correct as compared to chance (50%). * denotes significantly ($p < .05$) different from chance

4 | DISCUSSION

This study is the first to demonstrate physiologic and behavioral effects of single-element focused ultrasound for noninvasive, thalamic neuromodulation in humans. The P14 SEP derived from median nerve stimulation showed a strong attenuation in both the peak-to-peak analysis and the time series analysis. This inhibition was accompanied by a decrease in ability of participants to discriminate difficult threshold tactile judgements while receiving tFUS. The thalamic modulation also resulted in inhibition of time windows later in the SEP though effect upon specific SEP potential amplitude was lacking. It is unclear from this data if thalamic modulation with tFUS translates to cortical changes. Despite equivocal findings in the later cortically sourced SEP, we found evidence of frequency inhibition in mostly beta and gamma power providing evidence for an effect upon cortical oscillatory dynamics similar to previous reports (Legon et al., 2014; Mueller et al., 2014). These data provide evidence that single element tFUS can be used to target subcortical structures in humans that effects physiological activity. Acoustic modeling that takes into consideration individual skull morphology demonstrated good conservation of the ultrasound beam characteristics from free water, however, the effect of skull should be considered in future studies of single-element focused ultrasound for deep brain stimulation in humans to ensure accurate targeting.

Despite evidence of EEG attenuation in the time series analysis in the time range commensurate with primary somatosensory cortex (SI) activity, the peak-to-peak analysis did not reveal an effect of tFUS on the N20/P27 complex sourced to SI area 3b (Allison et al., 1989a, 1989b), that is responsible for fine discrimination behavior (Recanzone, Merzenich, Jenkins, Grajski, & Dinse, 1992) which may explain equivocal behavioral results. We hypothesized that thalamic attenuation may translate to early SI effects via direct thalamocortical connectivity, but instead we found a cortical effect around 35 ms, that corresponds well to the N33 SEP, but this potential is likely not generated in area 3b (Allison et al., 1989a,b) and hence may not directly relate to fine discrimination behavior of the fingertip. Interestingly, the behavioral results are opposite to those we found earlier (Legon et al., 2014). In Legon et al. (2014), we directed tFUS at the posterior bank of the central sulcus to directly target the source of the N20/P27 SEP complex and despite finding an inhibition of the amplitude of this complex, we found an increase in tactile detection ability. Here, we found an inhibition of the P14 potential with a decrease in difficult threshold tactile judgements. The relationship between SEP amplitude and behavior is not clear though differing behavioral effects between these two studies is probably a result of the anatomical location of tFUS effect. Lesion of the thalamus including VPL affects discrimination ability, but only when presented in combination with competing stimuli (sensory extinction)

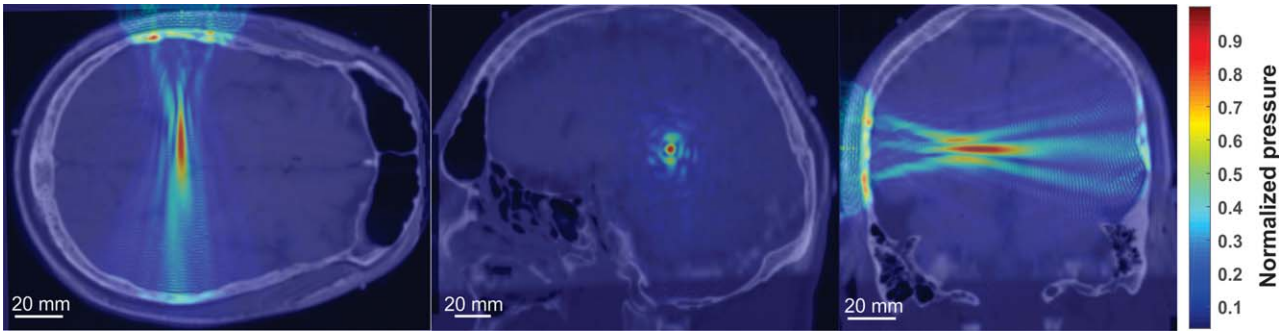

FIGURE 6 Acoustic modeling of ultrasound wave propagation. Normalized pseudocolor pressure distribution in a single subject acoustic model of ultrasound wave propagation using CT scan to account for the effect of skull morphology. Image shows MRI with CT overlay. Transducer is placed at the top of the transverse image (left) and on the left of the coronal image

and does not affect discrimination thresholds alone. Furthermore, recovery of this ability was related to the N20/P27 SEP amplitude recovery (Staines, Black, Graham, & McIlroy, 2002). The effect of thalamic lesion or attenuation seems to be more complex than simply disrupting information flow from the periphery and may involve attention or complex sensory gating mechanisms. This again, may explain our equivocal behavioral results where there wasn't a statistically significant difference between tFUS and sham conditions though evidence of impaired ability as compared to chance detection. We are confident this is not due to gross attentional factors or response bias as participants performed catch trials and easy discriminations with high success under both conditions. Further thorough exploration of the behavioral effect of subcortical tFUS neuromodulation perhaps under a similar paradigm to Staines et al., (2002) may help to elucidate a significant behavioral effect.

The effect of tFUS on the frequency spectra of the EEG supports our previous findings of an attenuation of EEG spectra (Legon et al., 2014) though here we showed time independent effects mainly in the beta frequency range. This is perhaps not too surprising as oscillatory activity as recorded from surface EEG is mainly the result of cortical activity (Wang, 2010). What is evident however from the wavelet convolution is strong time-locked gamma modulation. Our previous results also showed this time-locked gamma inhibition that can change in time depending upon location of neuromodulation. Gamma activity may represent cortical activity responsible for the initial encoding of a sensory stimulus (Fukuda et al., 2008; Tallon-Baudry & Bertrand, 1999) or may index attention to the stimulus (Fries, 2009) which would fit with the work of Staines et al. (2002) and Guillery, Feig, and Lozsadi (1998) that the thalamus is not just a passive relay of information but rather a complex attentional gating mechanism.

5 | LIMITATIONS AND CONSIDERATIONS

The skull represents the primary barrier to ultrasound due to its high frequency dependent attenuation, dispersion, and refraction of ultrasound waves which results in a significant loss of energy and distortion of the transmitted ultrasound beam. Our previous work using computational modelling of neuromodulatory transcranial focused ultrasound using a simplified skull found the inclusion of brain tissues and geometry to have little impact on transcranial pressure maps and to result in safe levels of heating in the skull and brain tissue [11]. However, changing the simplified skull geometry from flat to curved reduced peak intensity by 40%. In Legon et al. (2014), we also confirmed the influence of skull on intracranial acoustic pressure to drop three- to fourfold and here, using a different skull sample and different transducer found a six- to sevenfold loss of intensity intracranially, affirming the skull as the major determinant of intracranial acoustic pressure. In addition to affecting intracranial acoustic pressure, the skull also can have a significant effect on the wave propagation. Previously, in a simplified computer model, we showed that curving the skull resulted in a defocusing of the peak effects of ultrasound that well approximated empirical observations (Mueller et al., 2016). This skull curvature increased the full-width half-maximum and translated the centroid in the axial direction away from the face of the transducer. In empirical acoustic tank observations in Legon et al. (2014), we showed an opposite effect, whereby, translation of the ultrasound wave through hydrated human cranium actually served to focus the ultrasound beam both laterally and axially. Thus, the skull looks to have variable effects on acoustic wave propagation and beam geometry likely dependent upon individual morphology but always results in pressure attenuation as compared to free water observations, the degree to which is dependent upon both the skull section and the ultrasound transducer and its placement. Here, we extend these findings using a detailed acoustic model with an individual CT image to show a case of the effect of temporal bone transmission on ultrasound wave propagation. This model displayed a very good representation to empirical observations though there is noticeable difference from free water. As such, computational models that take into account individual skull morphology are warranted for accurate beam location and intensity. Detailed computational models of the skull are used in applications including aberration correction in high intensity focused ultrasound for thermal ablation (Marquet et al., 2009) and nonthermal ablation with microbubble enhanced focused ultrasound (Top, White, & McDannold, 2016). We were not able to acquire CT scans of the participants in this study and given the initial model shown here (despite a good conservation of beam geometry) it is recommended for future subcortical single-element transcranial ultrasound studies that CT scans of individuals are acquired and detailed computational models run to ensure accurate target localization and transducer placement (Mueller et al. 2017). This may not be feasible in some cases or not recommended to expose participants to unnecessary ionizing radiation. As such, ultrashort TE MRI may be a realistic alternative for accurate imaging of bone (Su et al., 2015) that can produce pseudo-CTs that could be used for accurate modeling of individual bone morphology.

One of the limitations of single-element ultrasound is the capacity for achieving volumes small enough to isolate (in this case) individual nuclei of the thalamus. The modeled beam for the transducer used in this study has an *x*-axis FWHM of 3.6 mm, *y*-axis FWHM of 3.6 mm, and a *z*-axis FWHM of 19.6 mm corresponding to an approximate FWHM volume of 133 mm^3. This volume is in good correspondence with the 50% probability map of sensory nuclei of thalamus volume of $\sim$160 mm^3 as taken from diffusion imaging in Behrens et al. (2003) and the lateral resolution is suitable for individual nuclei targeting though the axial resolution as used here would be larger than VPL. These volumes would also be commensurate with other subcortical structures such as the striatum (Yin et al., 2009) and hippocampus (Bremner et al., 2000) for instance. Of particular importance when employing single element ultrasound for deep brain neuromodulation is the potential for sonicating regions in close proximity to the intended target or regions along the axial path intermediate to the source and target (as well as beyond) due to the relatively large axial acoustic field produced by a single element as compared to a phased array for example as used in thalamotomy surgeries for essential tremor (Elias et al. 2013). It is possible that other parts of the thalamus like the reticular nucleus or more

medial portions of thalamus and perhaps the internal capsule and/or portions of the basal ganglia including the external globus pallidus or putamen were subject to sonication intensities sufficient for neuromodulation in this study. The effect of this inadvertent neuromodulation could contribute to our results, especially those outside of the P14 as the thalamus has rich inter connectivity to cortex and is involved in many dynamic processes for information relay to cortex (Sherman & Guillery, 1996). Internal capsule modulation could be examined with motor cortical stimulation though recent work has demonstrated ultrasound effects on nerve bundles to be significantly correlated to inertial cavitation (Wright, Haqshenas, Rothwell, & Saffari, 2017) that is unlikely here due to the low intensity used. Unfortunately, the absolute acoustic intensity necessary for human neuromodulation is not yet expressly known and thus it is difficult to say if these structures, despite laying outside the beam maxima, could have been modulated. Further research should work to determine ALARA (as low as reasonably achievable) principles for human acoustic neuromodulation to help determine if other structures are being modulated. These issues can be partly mitigated by tightening the ultrasound field though this has limitations. The spatial resolution of the ultrasonic field can be controlled and is largely determined by the acoustic frequency and the ratio of the focal length to the aperture of the transducer (referred to as the *f*-number). These characteristics can be manipulated to achieve a desired focal volume though practical consideration limits the applicability of some of these. Higher frequencies would result in shorter wavelengths and thus improved resolution though frequencies below 700 kHz are optimal for transcranial transmission where higher frequencies experience very high attenuation (White, Clement, & Hynynen, 2006). Given a set radius of curvature (focal length), a larger aperture single element transducer could also be employed to reduce the focal volume of acoustic pressure, however, very large aperture transducers would be difficult to effectively couple to the head. For example, this would likely be the case if a volume roughly one-half the 50% probability map size ($\sim$80 mm^3) of sensory nuclei in thalamus is desirable at a focal length of 55 mm as this would necessitate an active element diameter of 70 mm at 0.5 MHz. Thus, depending on the desired spatial volume, single element focused ultrasound for deep subcortical neuromodulation (near the center of the head) in humans is likely limited to volumes $\geq$150 mm^3 and an axial resolution of $\sim$20 mm. The use of multielement arrays is therefore necessary to achieve small volumes at deep focal lengths as is employed in high-intensity focused ultrasound (HIFU) applications for thalamotomy for example (Elias et al., 2013; Lipsman et al., 2013). Despite the volume and axial resolution limitations of a single element, focused ultrasound has the ability to target subcortical human anatomy that conventional electric and electromagnetic methods cannot currently achieve (Deng et al., 2014; Opitz et al., 2016). For cortical stimulation, focused ultrasound remains an unparalleled method for achieving very small, focal volumes. The FWHM area can be controlled to very small volumes ($\sim$25 mm^3) at focal lengths ($\sim$30 mm) suitable for human cortical stimulation. An additional consideration for single-element focused ultrasound for human neuromodulation is the coupling mechanism and the stability of this coupling. Degassed, deionized water is ideal to prevent the formation of gas bodies, though, depending on the size of the transducer and the location on the scalp may not always be feasible. Here, and in previous studies, we have used acoustic coupling gels that work well though are susceptible to air bubbles that could affect intensity and beam geometry. The amount of hair between the transducer and the scalp is also potentially limiting as this has the capacity to trap air bubbles as well. Efforts to carefully part the hair to establish good coupling are necessary and data on the effectiveness of this under different coupling conditions (hair and gel as compared to degassed water) should be conducted to provide quantitative assessment of this effect in future applications to ensure accurate reported intracranial intensities.

Finally, the safety of ultrasound for human neuromodulation is of paramount importance. Despite theoretical hypotheses of the exact bioeffect of transcranial focused ultrasound for neuromodulation (Krasovitski, Frenkel, Shoham, & Kimmel, 2011; Tyler, 2012), adherence to the recommendations of the Food and Drug Administration (FDA) regulations for diagnostic ultrasound are recommended. The FDA has set limits for carrier waves above 1MHz to a spatial peak pulse average (I_{sppa}) of 190 W/cm^2 and a mechanical index (MI = peak negative pressure/$\sqrt{fc}$) of 1.9. MI is an indication of the ability to produce cavitation related bioeffects and can be used as an indication for potential micromechanical damage. We are careful to restrict the intensity and MI well below these limits. We also employ a pulsing strategy using a broadband sharply focused transducer to avoid the generation of standing waves as recommended by O'Brien (2007). We have previously demonstrated that waveforms similar to those used here and in previous human neuromodulation applications do not produce appreciable tissue heating Mueller et al. (2016). However, ultrasound at higher intensities or during long exposures can cause tissue damage. Recently, Lee et al. (2016c) showed that low intensity ultrasound ($\sim$6 W/cm^2) delivered at close interstimulus interval (1 s) for 600 stimulations resulted in observable micro tissue damage in sheep. The sequela of this is not well understood as the animal in this instance did not present with any neurological or behavioral symptoms prior to histological examination. Despite this, this is an important finding as the intensity used (6 W/cm^2) is very low and similar to those employed in human studies (Lee et al., 2015, 2016b; Legon et al., 2014; Mueller et al., 2014) thus speaking to the ability of not just intensity, but repetition rate and total exposure per unit time to cause potential tissue damage. The authors also reported that an animal that received a single 100 stimuli session at an ISI of 1s did not show any histological results. As such, mechanical damage may be related to some relationship between intensity, ISI, and total number of sonications. Further large animal studies addressing this would prove valuable to the field to determine this relationship. In a recent swine study, Dallapiazza et al. (2017) used 1.15 MHz single element focused ultrasound directed at the ventral posterior lateral nucleus of thalamus at an I_{sppa} of 25 W/cm^2 for 40 s using a 100 ms pulsing scheme with a 43.7% duty cycle and did not observe any histological damage in all eight animals tested. This is a slightly different

pulsing scheme as has been employed in previous human studies though is a higher intensity and a longer single trial exposure. As with any energy modality, ultrasound can cause tissue damage, so caution should be used in the employment of ultrasound for noninvasive human brain neuromodulation.

6 | CONCLUSIONS

The results from this study provide initial evidence that single-element focused ultrasound can be targeted with good spatial precision and resolution to noninvasively modulate subcortical areas of the human brain. Further work establishing how these effects explicitly transfer to cortical functioning and behavior is necessary to fully characterize ultrasound for deep brain neuromodulation. For these purposes, inclusion of models that take individual skull morphology into consideration are warranted to produce accurate intensity levels and targeting. It is widely agreed that such a tool could bring revolutionary advances in neuroscience as it would enable unprecedented noninvasive functional mapping and neuromodulation of the whole human brain.

ACKNOWLEDGMENTS

This work was supported by the Wallin Neuroscience Discovery Fund. The authors would like to thank Jeff Elias for help with a previous version of this manuscript. Modeling performed in this manuscript was performed using resources provided by the Minnesota Supercomputing Institute (MSI) at the University of Minnesota http://www.msi.umn.edu.

ORCID

Wynn Legon http://orcid.org/0000-0002-8761-3496

REFERENCES

Allison, T., McCarthy, G., Wood, C. C., Darcey, T. M., Spencer, D. D., & Williamson, P. D. (1989a). Human cortical potentials evoked by stimulation of the median nerve. I. Cytoarchitectonic areas generating short-latency activity. *Journal of Neurophysiology*, *62*, 694–710.

Allison, T., McCarthy, G., Wood, C. C., & Jones, S. J. (1991). Potentials evoked in human and monkey cerebral cortex by stimulation of the median nerve. A review of scalp and intracranial recordings. *Brain*, *114*(Pt 6), 2465–2503.

Allison, T., McCarthy, G., Wood, C. C., Williamson, P. D., & Spencer, D. D. (1989b). Human cortical potentials evoked by stimulation of the median nerve. II. Cytoarchitectonic areas generating long-latency activity. *Journal of Neurophysiology*, *62*, 711–722.

Aubry, J. F., Tanter, M., Pernot, M., Thomas, J. L., & Fink, M. (2003). Experimental demonstration of noninvasive transskull adaptive focusing based on prior computed tomography scans. *The Journal of the Acoustical Society of America*, *113*, 84–93.

Behrens, T. E., Johansen-Berg, H., Woolrich, M. W., Smith, S. M., Wheeler-Kingshott, C. A., Boulby, P. A., … Matthews, P. M. (2003). Non-invasive mapping of connections between human thalamus and cortex using diffusion imaging. *Nature Neuroscience*, *6*, 750–757.

Beissner, K. (1982). On the plane-wave approximation of acoustic intensity. *The Journal of the Acoustical Society of America*, *71*, 1406.

Bremner, J. D., Narayan, M., Anderson, E. R., Staib, L. H., Miller, H. L., & Charney, D. S. (2000). Hippocampal volume reduction in major depression. *The American Journal of Psychiatry*, *157*, 115–118.

Connor, C. W. (2003). *Simulation methods and tissue property models for non-invasive transcranial focused ultrasound surgery*. Cambridge: Massachusetts Institute of Technology.

Dallapiazza, R. F., Timbie, K. F., Holmberg, S., Gatesman, J., Lopes, M. B., Price, R. J., Miller, G. W., & Elias, W. J. (2017). Noninvasive neuromodulation and thalamic mapping with low-intensity focused ultrasound. *Journal of Neurosurgery*, 1–10.

Deffieux, T., Younan, Y., Wattiez, N., Tanter, M., Pouget, P., & Aubry, J. F. (2013). Low-intensity focused ultrasound modulates monkey visuomotor behavior. *Current Biology*, *23*, 2430–2433.

Deng, Z. D., Lisanby, S. H., & Peterchev, A. V. (2014). Coil design considerations for deep transcranial magnetic stimulation. *Clinical Neurophysiology*, *125*, 1202–1212.

Downs, M. E., Buch, A., Karakatsani, M. E., Konofagou, E. E., & Ferrera, V. P. (2015). Blood-brain barrier opening in behaving non-human primates via focused ultrasound with systemically administered microbubbles. *Scientific Reports*, *5*, 15076.

Elias, W. J., Huss, D., Voss, T., Loomba, J., Khaled, M., Zadicario, E., … Wintermark, M. (2013). A pilot study of focused ultrasound thalamotomy for essential tremor. *The New England Journal of Medicine*, *369*, 640–648.

Fries, P. (2009). Neuronal gamma-band synchronization as a fundamental process in cortical computation. *Annual Review of Neuroscience*, *32*, 209–224.

Fukuda, M., Nishida, M., Juhasz, C., Muzik, O., Sood, S., Chugani, H. T., & Asano, E. (2008). Short-latency median-nerve somatosensory-evoked potentials and induced gamma-oscillations in humans. *Brain: A Journal of Neurology*, *131*, 1793–1805.

Gavrilov, L. R. (2016). Focused ultrasound stimulation of the peripheral nervous system: Physical basis and practical applications. *International Journal of Modern Physics: Advances in Theory and Application*, *1*, 45–118.

Guillery, R. W., Feig, S. L., & Lozsadi, D. A. (1998). Paying attention to the thalamic reticular nucleus. *Trends in Neurosciences*, *21*, 28–32.

Katayama, Y., & Tsubokawa, T. (1987). Somatosensory evoked potentials from the thalamic sensory relay nucleus (VPL) in humans: Correlations with short latency somatosensory evoked potentials recorded at the scalp. *Electroencephalography and Clinical Neurophysiology*, *68*, 187–201.

Kim, H., Chiu, A., Lee, S. D., Fischer, K., & Yoo, S. S. (2014). Focused ultrasound-mediated non-invasive brain stimulation: Examination of sonication parameters. *Brain Stimulation*, *7*, 748–756.

King, R. L., Brown, J. R., Newsome, W. T., & Pauly, K. B. (2013). Effective parameters for ultrasound-induced in vivo neurostimulation. *Ultrasound in Medicine &Amp; Biology*, *39*, 312–331.

Krasovitski, B., Frenkel, V., Shoham, S., & Kimmel, E. (2011). Intramembrane cavitation as a unifying mechanism for ultrasound-induced bioeffects. *Proceedings of the National Academy of Sciences of the United States of America*, *108*, 3258–3263.

Lee, W., Chung, Y. A., Jung, Y., Song, I. U., & Yoo, S. S. (2016a). Simultaneous acoustic stimulation of human primary and secondary somatosensory cortices using transcranial focused ultrasound. *BMC Neuroscience*, *17*, 68.

Lee, W., Kim, H., Jung, Y., Song, I. U., Chung, Y. A., & Yoo, S. S. (2015). Image-guided transcranial focused ultrasound stimulates human primary somatosensory cortex. *Scientific Reports*, *5*, 8743.

Lee, W., Kim, H. C., Jung, Y., Chung, Y. A., Song, I. U., Lee, J. H., & Yoo, S. S. (2016b). Transcranial focused ultrasound stimulation of human primary visual cortex. *Scientific Reports*, *6*, 34026.

Lee, W., Lee, S. D., Park, M. Y., Foley, L., Purcell-Estabrook, E., Kim, H., … Yoo, S. S. (2016c). Image-guided focused ultrasound-mediated

regional brain stimulation in sheep. *Ultrasound in Medicine &Amp; Biology*, *42*, 459–470.

Legon, W., Sato, T. F., Opitz, A., Mueller, J., Barbour, A., Williams, A., & Tyler, W. J. (2014). Transcranial focused ultrasound modulates the activity of primary somatosensory cortex in humans. *Nature Neuroscience*, *17*, 322–329.

Lipsman, N., Schwartz, M. L., Huang, Y., Lee, L., Sankar, T., Chapman, M., … Lozano, A. M. (2013). MR-guided focused ultrasound thalamotomy for essential tremor: A proof-of-concept study. *The Lancet. Neurology*, *12*, 462–468.

Maris, E., & Oostenveld, R. (2007). Nonparametric statistical testing of EEG- and MEG-data. *Journal of Neuroscience Methods*, *164*, 177–190.

Marquet, F., Pernot, M., Aubry, J. F., Montaldo, G., Marsac, L., Tanter, M., & Fink, M. (2009). Non-invasive transcranial ultrasound therapy based on a 3D CT scan: Protocol validation and in vitro results. *Physics in Medicine and Biology*, *54*, 2597–2613.

Mehic, E., Xu, J. M., Caler, C. J., Coulson, N. K., Moritz, C. T., & Mourad, P. D. (2014). Increased anatomical specificity of neuromodulation via modulated focused ultrasound. *PLoS One*, *9*, e86939.

Min, B. K., Bystritsky, A., Jung, K. I., Fischer, K., Zhang, Y., Maeng, L. S., … Yoo, S. S. (2011). Focused ultrasound-mediated suppression of chemically-induced acute epileptic EEG activity. *BMC Neuroscience*, *12*, 23–2202-12–23.

Monti, M. M., Schnakers, C., Korb, A. S., Bystritsky, A., & Vespa, P. M. (2016). Non-invasive ultrasonic thalamic stimulation in disorders of consciousness after severe brain injury: A first-in-man report. *Brain Stimulation*, *9*, 940–941.

Moore, M. E., Loft, J. M., Clegern, W. C., & Wisor, J. P. (2015). Manipulating neuronal activity in the mouse brain with ultrasound: A comparison with optogenetic activation of the cerebral cortex. *Neuroscience Letters*, *604*, 183–187.

Mueller, J., Legon, W., Opitz, A., Sato, T. F., & Tyler, W. J. (2014). Transcranial focused ultrasound modulates intrinsic and evoked EEG dynamics. *Brain Stimulation*, *7*, 900–908.

Mueller, J. K., Ai, L., Bansal, P., & Legon, W. (2016). Computational exploration of wave propagation and heating from transcranial focused ultrasound for neuromodulation. *Journal of Neural Engineering*, *13*. Epub 2016 Jul 28.

Mueller, J. K., Ai, L., Bansal, P., & Legon, W. (2017). Numerical evaluation of the skull for human neuromodulation with transcranial focused ultrasound. *Journal of Neural Engineering*.

O'Brien, W. D. Jr (2007). Ultrasound-biophysics mechanisms. *Progress in Biophysics and Molecular Biology*, *93*, 212–255.

Opitz, A., Falchier, A., Yan, C. G., Yeagle, E. M., Linn, G. S., Megevand, P., … Schroeder, C. E. (2016). Spatiotemporal structure of intracranial electric fields induced by transcranial electric stimulation in humans and nonhuman primates. *Scientific Reports*, *6*, 31236.

Pinkerton, J. M. M. (1949). The absorption of ultrasonic waves in liquids and its relation to molecular constitution. *Proceedings of the Physical Society. Section B*, *62*.

Preston, R. C. (1986). Measurement and characterisation of the acoustic output of medical ultrasonic equipment. Part 1. *Medical &Amp; Biological Engineering &Amp; Computing*, *24*, 113–120.

Recanzone, G. H., Merzenich, M. M., Jenkins, W. M., Grajski, K. A., & Dinse, H. R. (1992). Topographic reorganization of the hand representation in cortical area 3b owl monkeys trained in a frequency-discrimination task. *Journal of Neurophysiology*, *67*, 1031–1056.

Rossi, S., Hallett, M., Rossini, P. M., & Pascual-Leone, A. Safety of TMS Consensus Group (2009). Safety, ethical considerations, and application guidelines for the use of transcranial magnetic stimulation in clinical practice and research. *Clinical Neurophysiology*, *120*, 2008–2039.

Sherman, S. M., & Guillery, R. W. (1996). Functional organization of thalamocortical relays. *Journal of Neurophysiology*, *76*, 1367–1395.

Spitzer, V. M., & Whitlock, D. G. (1998). The Visible Human Dataset: The anatomical platform for human simulation. *The Anatomical Record*, *253*, 49–57.

Staines, W. R., Black, S. E., Graham, S. J., & McIlroy, W. E. (2002). Somatosensory gating and recovery from stroke involving the thalamus. *Stroke*, *33*, 2642–2651.

Su, K. H., Hu, L., Stehning, C., Helle, M., Qian, P., Thompson, C. L., … Traughber, B. J. (2015). Generation of brain pseudo-CTs using an undersampled, single-acquisition UTE-mDixon pulse sequence and unsupervised clustering. *Medical Physics*, *42*, 4974–4986.

Tallon-Baudry, C., & Bertrand, O. (1999). Oscillatory gamma activity in humans and its role in object representation. *Trends in Cognitive Sciences*, *3*, 151–162.

Top, C. B., White, P. J., & McDannold, N. J. (2016). Nonthermal ablation of deep brain targets: A simulation study on a large animal model. *Medical Physics*, *43*, 870–882.

Treeby, B. E., & Cox, B. T. (2010). k-Wave: MATLAB toolbox for the simulation and reconstruction of photoacoustic wave fields. *Journal of Biomedical Optics*, *15*, 021314.

Tufail, Y., Matyushov, A., Baldwin, N., Tauchmann, M. L., Georges, J., Yoshihiro, A., … Tyler, W. J. (2010). Transcranial pulsed ultrasound stimulates intact brain circuits. *Neuron*, *66*, 681–694.

Tyler, W. J. (2012). The mechanobiology of brain function. *Nature Reviews. Neuroscience*, *13*, 867–878.

Wang, X. J. (2010). Neurophysiological and computational principles of cortical rhythms in cognition. *Physiological Reviews*, *90*, 1195–1268.

White, P. J., Clement, G. T., & Hynynen, K. (2006). Local frequency dependence in transcranial ultrasound transmission. *Physics in Medicine and Biology*, *51*, 2293–2305.

Wright, C. J., Haqshenas, S. R., Rothwell, J., & Saffari, N. (2017). Unmyelinated peripheral nerves can be stimulated in vitro using pulsed ultrasound. *Ultrasound in Medicine &Amp; Biology*, *43*, 2269–2283.

Yang, P. S., Kim, H., Lee, W., Bohlke, M., Park, S., Maher, T. J., & Yoo, S. S. (2012). Transcranial focused ultrasound to the thalamus is associated with reduced extracellular GABA levels in rats. *Neuropsychobiology*, *65*, 153–160.

Yin, D., Valles, F. E., Fiandaca, M. S., Forsayeth, J., Larson, P., Starr, P., & Bankiewicz, K. S. (2009). Striatal volume differences between nonhuman and human primates. *Journal of Neuroscience Methods*, *176*, 200–205.

Yoo, S. S., Bystritsky, A., Lee, J. H., Zhang, Y., Fischer, K., Min, B. K., … Jolesz, F. A. (2011). Focused ultrasound modulates region-specific brain activity. *NeuroImage*, *56*, 1267–1275.

SUPPORTING INFORMATION

Additional Supporting Information may be found online in the supporting information tab for this article.

How to cite this article: Legon W, Ai L, Bansal P, Mueller JK. Neuromodulation with single-element transcranial focused ultrasound in human thalamus. *Hum Brain Mapp*. 2018;39:1995–2006. https://doi.org/10.1002/hbm.23981